

A homologous recycling model for hot galactic coronae

Alexei G. Kritsuk^{1,2,3*}

¹ *Institute of Astronomy, University of St. Petersburg, Stary Peterhof, St. Petersburg 198904, Russia*

² *Max-Planck-Institut für Astrophysik, Postfach 1523, D-85740 Garching, Germany*

³ *Max-Planck-Institut für extraterrestrische Physik, Postfach 1603, D-85740 Garching, Germany*

Accepted 1995 December 11. Received 1995 July 6; in original form 1995 January 3

ABSTRACT

An equilibrium model is presented for a hydrostatic isothermal hot gas distribution in a gravitational well of a giant elliptical galaxy immersed in a massive dark halo. The self-consistently determined gravitational potential of the system provides the optical surface brightness distribution of the galaxy, matching the de Vaucouleurs $R^{1/4}$ -law, if the sound speed in the gas c , stellar velocity dispersion σ_* , and velocity dispersion of dark matter σ_{DM} are related by $\sigma_{\text{DM}} \simeq c \simeq \sqrt{2}\sigma_*$. While the first equality follows from virial considerations, the second one relies on the observed similarity of optical and X-ray brightness profiles. The thermal equilibrium of the gas is described in the framework of a one-zone model, which incorporates radiative cooling, stellar mass loss, supernova heating, and mass sink due to local condensational instability. The sequence of *saddle-node* and *saddle-connection* bifurcations provides a first-order phase transition, which separates the stable hot phase in the cooling medium for a reasonably high efficiency of condensation and precludes catastrophic cooling of the gas. The bifurcations occur naturally, due to the shape of the radiative cooling function, and this holds for a wide range of gas metallicities. The one-zone model implies a scaling relation for the equilibrium stellar and gas densities $\rho_* \propto \rho^2$, which allows a hydrostatic, thermally stable distribution for the hot isothermal coronal gas. The resulting homologous recycling model reproduces the basic optical and X-ray properties of relatively isolated giant elliptical galaxies with hot haloes. Implications for cD galaxies in X-ray dominant clusters and groups are briefly discussed in the general context of galaxy formation and evolution.

Key words: hydrodynamics – instabilities – cooling flows – galaxies:ISM – X-rays:ISM – X-rays:galaxies

1 INTRODUCTION

The analysis of the extended X-ray emission of early-type galaxies has led to an extension of the cooling flow model [see Fabian, Nulsen & Canizares (1984) and Fabian (1994)] applied to the class of bright elliptical galaxies (Thomas et al. 1986). The typical X-ray luminosities of such galaxies are in the range $10^{39} - 10^{42}$ erg s⁻¹, the gas temperature is $5 \times 10^6 - 2 \times 10^7$ K, and the electron number density in the centre is $0.01 - 0.1$ cm⁻³. The galaxies usually contain $10^9 - 10^{10} M_\odot$ of the gas in their extended hot haloes (Forman, Jones & Tucker 1985). Observations reveal a tight connection of X-ray and optical characteristics of the galaxies, including a strong correlation between the X-ray and optical luminosities, although with a considerable scatter (Canizares et al. 1987; Donnelly et al. 1990), and a sim-

ilarity of X-ray and optical light distributions (Trinchieri, Fabbiano & Canizares 1986; Killeen & Bicknell 1988).

The source of the gas in hot haloes of early-type galaxies is usually attributed to the normal stellar mass loss with a specific rate $\dot{\rho}_*/\rho_* \sim 1 - 2 \times 10^{-12}$ yr⁻¹. Gas injection from stars and supernova events in the galaxy make the gas inhomogeneous (Mathews 1990) and thermal instability causes matter to cool out at radii $r < r_{\text{cool}}$, where $t_{\text{cool}} < H_0^{-1}$ (Nulsen 1986). The dynamics of the gas, therefore, is determined by the relative rates of the processes, controlling its mass and energy balance. Theoretical work done so far has demonstrated a variety of possible behaviours for the gas, ranging from supersonic galactic winds to subsonic inflows [see Thomas (1986), Hattori, Habe & Ikeuchi (1987), David, Forman & Jones (1990), Ciotti et al. (1991) and references therein]. However, due to the non-linear nature of radiative cooling, numerical modelling of inflows usually ends up with a cooling catastrophe in the centre of the galaxy, which overproduces the observed X-rays and precludes the study

* E-mail: agk@aispbu.spb.su

of further evolution. As there are no certain observational indications of such a catastrophe, it is important to understand the nature of possible physical damping mechanisms, which are able to prevent it.

It is an objective of this paper to present a purely hydrostatic, thermodynamically stable model for gas recycling in an elliptical galaxy, which satisfies the observational constraints. The model incorporates all the same physical processes as the ‘standard’ multiphase cooling flow model, and may also be useful in interpreting the X-ray emission from the central ‘cooling flow’ regions in dynamically quiet X-ray dominant clusters or groups, where the outskirts of the central dominant optical galaxy extend to the cooling radius.

2 UNDERLYING GALAXY MODEL

Let $M(r)$ be a spherically symmetric configuration of the gravitating mass, including the stellar component of a galaxy, the hot gas, and the dark halo. Then the hydrostatic gas distribution in the gravitational potential $\phi(r)$ of $M(r)$ can be described by

$$\frac{kT}{\mu m_p} \left(\frac{d \ln \rho}{dr} + \frac{d \ln T}{dr} \right) = -\nabla \phi \equiv -\frac{GM(r)}{r^2}. \quad (1)$$

For the isothermal gas this reduces to

$$\frac{kT}{\mu m_p} \frac{d \ln \rho}{dr} = -\nabla \phi. \quad (2)$$

Here T and ρ are the gas temperature and density, μ the mean molecular weight, m_p the proton mass, and k Boltzmann’s constant.

The stellar density distribution of the galaxy, ρ_* , responding to the same gravitational potential, satisfies

$$\sigma_r^2 \left(\frac{d \ln \rho_*}{dr} + \frac{d \ln \sigma_r^2}{dr} + \frac{2\eta}{r} \right) = -\nabla \phi, \quad (3)$$

where σ_r is the radial velocity dispersion of stars in the galaxy, the anisotropy parameter η is defined as $\eta = 1 - \sigma_t^2/\sigma_r^2$, and the subscript ‘t’ represents the tangential velocity component. In the case of an isotropic and uniform stellar velocity distribution ($\sigma_t = \sigma_r \equiv \text{const}$) it simply follows that

$$\sigma_*^2 \frac{d \ln \rho_*}{dr} = -\nabla \phi, \quad (4)$$

where σ_* is the one-dimensional velocity dispersion. For an isothermal gas and an isotropic, constant stellar velocity dispersion the stellar and gas densities are related as

$$\frac{d \ln \rho}{d \ln \rho_*} = \frac{\mu m_p \sigma_*^2}{kT} = \frac{\sigma_*^2}{c^2} \equiv \beta, \quad (5)$$

or

$$\rho = C \rho_*^\beta, \quad (6)$$

where c is the isothermal sound speed and C is the integration constant. This relation provides the basis for the so-called isothermal β -model (Cavaliere & Fusco-Femiano 1976), extensively used to describe the X-ray surface brightness of the hot gas in clusters of galaxies.

Given equation (6) and assuming similar profiles for the gas density ρ and for the dark matter density ρ_{DM} (and,

therefore, $\sigma_{DM} = c$)[†], one can define the total mass distribution self-consistently, using Poisson’s equation

$$\frac{1}{r^2} \frac{d}{dr} \left(r^2 \frac{d \ln \rho_*}{dr} \right) = -\frac{4\pi G}{\sigma_*^2} (\rho_* + \rho + \rho_{DM}). \quad (7)$$

When $\beta \simeq 1/2$ and in the centre $\rho_{*,0}$ is somewhat higher than $\rho_{DM,0}$, the stellar system has a density distribution which is similar to the profile of a self-gravitating isothermal sphere, but has a density cut-off at the core radius of the dark matter halo, where the dark matter density begins to fall as $\rho_{DM} \propto r^{-2}$, cf. Burkert (1994). It turns out that such a solution of (7) gives the projected stellar mass density, which follows the de Vaucouleurs $R^{1/4}$ -law over several orders of magnitude in surface brightness, in a wide range of radii $0.1R_e \leq r \leq 1.5R_e$, where R_e is the effective radius (Burkert 1994). This can be expected if the stellar system formed in a dissipative process from post-infall shock heated gas with the star formation rate $\propto \rho^2$.

The volume density of the $\beta = 1/2$ stellar system falls more steeply than $\rho_* \propto r^{-2}$ outside the core region (Burkert 1994), therefore the restriction on stellar velocity dispersion, imposed to derive (6), can be formulated as

$$\left| \frac{d \ln \sigma_*}{d \ln r} + \eta \right| \ll 1, \quad (8)$$

while the gas must be isothermal up to

$$\left| \frac{d \ln T}{d \ln r} \right| \ll 1. \quad (9)$$

Due to projection effects it is difficult to demonstrate whether the above conditions are indeed satisfied in observed systems or not. However, in most cases early-type galaxies do exhibit rather flat line-of-sight velocity dispersion profiles and observations also show that the gas is quite isothermal. The details of observational data will be briefly discussed in Section 5.

3 ONE-ZONE MODEL REVISITED

A simple semi-analytical one-zone model allows an insight into the non-linear thermodynamics of the hot gas in the halo of a galaxy. While the stability of gas equilibria was studied in Kritsuk (1992) with an emphasis on limit cycle solutions, considerations here concentrate mainly on classification of bifurcations, which lead to the separation of a stable hot phase of the thermally unstable cooling medium. In the following subsections the basic formulae of the model are compiled from Kritsuk (1992) in order to lead up to the bifurcation analysis. The only new physical process introduced is the feedback heating. It was neglected before, but may play an important role in highly non-equilibrium situations.

[†] The approximate equality of the dark matter velocity dispersion and the sound velocity of the gas has been demonstrated, e.g. by the simulations of X-ray clusters of galaxies in the cold dark matter cosmogony for those clusters that are not merging objects, experiencing a transient boost in the velocity dispersion of the system (Navarro, Frenk & White 1995).

3.1 Input physics

The set of physical processes incorporated in cooling flow models includes radiative cooling, mass deposition due to thermal instabilities, supernova (SN) type Ia heating, and stellar mass loss for the galaxy, which is immersed in a dark halo. Here only the basic formulae are presented; one can find more extensive discussion elsewhere [e.g. in Sarazin & White (1987), see also references below]. The standard notation is kept where possible.

3.1.1 Stellar mass loss

The efficiency of gas deposition due to stellar mass loss and SN Ia explosions is proportional to the stellar mass density: $\alpha\rho_*(r)$, where $\alpha = \alpha_* + \alpha_{\text{sn}} \equiv \text{const}$ incorporates contributions from more quiescent stellar mass loss $\alpha_* \simeq 4.7 \times 10^{-20} \text{ s}^{-1}$ (Faber & Gallagher 1976; Sarazin & White 1987), and mass loss by supernovae $\alpha_{\text{sn}} = 1.33 \times 10^{-21} \text{ s}^{-1}$ (the estimate corresponds to $r_{\text{sn}} = 0.24 h_{50}^2 \text{ SNU}$, $M_{\text{sn}} = 1.4 M_\odot$, and $(M/L_B)_* = 8M_\odot/L_\odot$). The supernova type Ia rate, r_{sn} , is uncertain by a factor of the order of 1.5 according to van den Bergh & Tammann (1991), where $h_{50} = H_0/50 \text{ km s}^{-1}\text{Mpc}^{-1}$, but a significantly lower estimate $r_{\text{sn}} = 0.06 \pm 0.03 h_{50}^2 \text{ SNU}$ is given by Turatto, Cappellaro & Benetti (1994).

3.1.2 Thermal instabilities

Drops of condensed material cool out from the hot gas because of thermal instabilities at the rate of $\dot{\rho}_{\text{ti}} = b\chi(n)\rho$, where the dimensionless parameter $b \equiv \text{const} \in [0, 1]$ controls the efficiency of condensation. The Heaviside function χ and the instability growth rate n are defined as

$$\chi(n) = \begin{cases} n, & \text{if } n \geq 0; \\ 0, & \text{otherwise;} \end{cases} \quad (10)$$

$$n \equiv \frac{\partial}{\partial t} \left(\ln \frac{\delta\rho}{\rho} \right) = \frac{1}{c_p} \left(\frac{2\rho\Lambda}{T} - \rho \frac{d\Lambda}{dT} \right) - \frac{\alpha\rho_*}{\rho}. \quad (11)$$

Here c_p is the specific heat at constant pressure, the first term in the rhs of equation (11) coincides with Field's instability criterion, and the second describes stabilization due to stellar mass loss (Kritsuk 1992). Note that if $\rho_* \propto \rho^2$, as in the $\beta = 1/2$ case, then $\dot{\rho}_{\text{ti}} \propto \rho^2$, which naturally implies a star formation rate from the cooled material proportional to the gas density squared.

3.1.3 Radiative cooling

Non-equilibrium radiative cooling as a function of temperature and metallicity, $\Lambda(T, Z) \text{ erg cm}^3 \text{ g}^{-2} \text{ s}^{-1}$, is compiled from the calculations of Sutherland & Dopita (1993), where solar abundance ratios were taken from Anders & Grevesse (1989). Effects of dust on the cooling are not taken into account here since the coronal phase is believed to be essentially dust-free. If the gas-to-dust ratio were similar to Galactic values, and the dust were well mixed in the hot interstellar medium, it could be the dominant cooling agent at gas temperatures above $2 \times 10^6 \text{ K}$ (Burke & Silk 1974). This would essentially change the shape of the cooling function and therefore the gas stability properties outlined below. A

crude estimate shows that dust cooling can be safely ignored if the dust content is $\lesssim 0.01$ of the Galactic value.

3.1.4 Heating

The rate of heating due to thermalization of stellar winds and due to type Ia SN events is assumed to be equal to $\alpha\rho_*T_0$, where T_0 is the characteristic temperature of the heat source, $T_0 = (\alpha_*T_* + \alpha_{\text{sn}}T_{\text{sn}})/\alpha$. Heating by stellar motions is described by $T_* = \mu m_p \sigma_*^2/k = 6.47 \times 10^6 \text{ K}$ (an estimate is made for $\sigma_* = 300 \text{ km s}^{-1}$), and SN temperature $T_{\text{sn}} = \frac{\mu m_p v_{\text{ej}}^2}{3k} = 1.09 \times 10^9 \text{ K}$ for $E_{\text{sn}} = 6 \times 10^{50} \text{ erg}$, $M_{\text{sn}} = 1.4 M_\odot$. With these values $T_0 \simeq 3.6 \times 10^7 \text{ K}$, while for $r_{\text{sn}} = 0.06 \text{ SNU}$ the source temperature is lower: $T_0 \simeq 1.7 \times 10^7 \text{ K}$.

3.1.5 Feedback heating

Energy feedback by type II (Ib) SN explosions due to star formation in cooled material can serve as an additional source of gas heating. This slightly modifies formulae for α and T_0 : $\alpha = \alpha_* + \alpha_{\text{sn}} + \alpha_{\text{fb}}$, where $\alpha_{\text{fb}} = \varepsilon_{\text{fb}}\dot{\rho}_{\text{ti}}$, $T_0 = (\alpha_*T_* + \alpha_{\text{sn}}T_{\text{sn}} + \alpha_{\text{fb}}T_{\text{fb}})/\alpha$. Here $T_{\text{fb}} = \frac{2\mu m_p E_{\text{th}}}{3kM_{\text{ej}}} = 3.6 \times 10^9 \text{ K}$, $E_{\text{th}} = 0.72E$ in the Sedov stage, and the supernova explosion energy $E = 2 \times 10^{51} \text{ erg}$. The optimistic estimate $\varepsilon_{\text{fb}} = 0.01$ is given in Silk et al. (1986), assuming a rate of type Ib SNe of 1 supernova yr^{-1} per $100 M_\odot \text{ yr}^{-1}$, and the mass of ejecta returned to the ISM $M_{\text{ej}} = 1 M_\odot$. The associated mass feedback is negligible, i.e. $\alpha \gg \varepsilon_{\text{fb}}\alpha$.

3.2 Basic equations

The mass and energy balance of the hot gas in the halo of a galaxy may be described locally by the autonomous set of ordinary differential equations:

$$\frac{d\rho}{dt} = \alpha\rho_* - \dot{\rho}_{\text{ti}}, \quad (12)$$

$$\frac{dT}{dt} = \frac{1}{\rho} [\alpha\rho_*(T_0 - T) - (\gamma - 1)\dot{\rho}_{\text{ti}}T - \rho^2\Lambda/c_v], \quad (13)$$

where t is the time variable and α , ρ_* , and T_0 are treated as constants; c_v is the specific heat at constant volume. The evolutionary solutions of equations (12) and (13) may be represented as trajectories in the (ρ, T) phase plane. The steady states of the system correspond to the fixed points and may be readily found as

$$\rho = \rho_{\text{eq}} c_0 \sqrt{\frac{\alpha\rho_*}{(\gamma - 1)\Lambda_0}}, \quad (14)$$

$$T = \Theta_{\text{eq}} T_0, \quad (15)$$

where $c_0 = c(T_0)$ is the isothermal sound speed, $\Lambda_0 = \Lambda(T_0, Z)$, metallicity Z is assumed to be constant, and ρ_{eq} and Θ_{eq} are dimensionless functions of b , T_0 , and Z :

$$\left(\frac{1}{\gamma\Theta_{\text{eq}}} - 1 \right) (2 - \nu_{\text{eq}}) = 1 + \frac{1}{b}, \quad (16)$$

$$\rho_{\text{eq}}^2 = (1 - \gamma\Theta_{\text{eq}})/\lambda_{\text{eq}}. \quad (17)$$

The subscript 'eq' denotes an equilibrium state, $\nu = d \ln \Lambda / d \ln T$, and $\lambda = \Lambda/\Lambda_0$.

The characteristic time-scale for evolution near the equilibrium,

$$t_s = \sqrt{t_{c0} t_\alpha}, \quad (18)$$

is a geometric mean of the local cooling time $t_{c0} \equiv c_0^2/[(\gamma - 1)\rho\Lambda_0]$ and the time-scale for stellar mass loss $t_\alpha = (\alpha\rho_*/\rho)^{-1}$.

For a given metallicity of the gas Z , stellar mass loss rate α , temperature of the heat source T_0 , and efficiency of condensation b , one can find the equilibrium solutions, if the cooling function is known. It is a straightforward piece of algebra then to classify these equilibria according to their stability properties, using the standard linear technique (see Kritsuk 1992). This analysis relies on poorly known high-order derivatives of Λ with respect to temperature and, therefore, the fine details of stability changes cannot be well resolved. At the same time, the main stability features, controlled by the nature of radiative cooling (resonance line emission, producing a prominent maximum in the range of temperatures $10^{4.2} \text{ K} \lesssim T \lesssim 10^{7.2} \text{ K}$, and thermal bremsstrahlung for $T \gtrsim 10^{7.2} \text{ K}$), do provide physically important effects, which are discussed in the next section.

3.3 First-order phase transition in a system with no feedback

The efficiency of condensation b is the only essentially free parameter of the model. It is important to understand how the equilibria and their stability follow the changes of this control parameter.

This is illustrated with a plot of the equilibrium temperature T_{eq} against b for a fixed value of the heat source temperature $T_0 = 3 \times 10^7 \text{ K}$ and solar metallicity (see Fig. 1). There are no steady-state solutions when the condensation efficiency is low, $b < b_1 = 0.0018$. The catastrophic cooling is unavoidable even in a system with reasonably strong SN heating. At $b = b_1$, as a result of a *fold* bifurcation, a *saddle-node* pair of fixed points appears simultaneously, providing stable and unstable steady-state solutions, classified as a *node* (higher temperature state) and a *saddle* (lower temperature state), respectively. The fold bifurcation is the simplest form of *local* bifurcation in that it requires only a one-dimensional phase space, only one control parameter, and only lowest-order terms (see, e.g., Guckenheimer & Holmes 1983; Thompson & Stewart 1989). It is *structurally stable* and, therefore, the small perturbation of the dynamics does not alter the bifurcation qualitatively. Equation (16) shows that the condensation efficiency b is a unique function of the equilibrium temperature Θ_{eq} and depends solely on the logarithmic temperature derivative of the cooling function ν_{eq} . Therefore the fold *catastrophe*[‡] occurs in the model due to the local structure of $\Lambda(T)$. As the control parameter becomes larger, multiple steady states appear and annihilate due to a series of bifurcations of the same kind. These further local changes in the phase portrait of the system at

$b_1 < b < 0.054$ are not so important because the new stable solutions have negligibly small *domains of attraction* (or basins) in the phase plane. The most essential event in the range of $b \in [0, 0.6]$ happens at $b = b_1$, where the first pair of fixed points spontaneously appears. Although these changes in the dynamics do not preclude the catastrophic cooling, the birth of the saddle leads up to further transformations in the system.

The next important event takes place at $b_2 = 0.092$ due to a spontaneous birth of a stable limit cycle. This is a *homoclinic connection* bifurcation or a *blue sky* catastrophe for a periodic limit cycle (Guckenheimer & Holmes 1983; Thompson & Stewart 1989). The blue sky catastrophe is a *global* bifurcation[§] in the phase plane in which the *attracting* limit cycle disappears (as b decreases) by collision with a saddle. The bifurcation is also structurally stable, that is, the full control-phase space diagram may be deformed, but qualitatively unchanged by small perturbations of the governing equations. At $b > b_2$ the basin of the attracting limit cycle grows, while the amplitude of non-linear temperature oscillations becomes smaller. As a result, at $b > 0.2$ only small-amplitude stable oscillations survive, which disappear at $b = b_3 = 0.427$ due to a supercritical Hopf bifurcation. Fig. 2 shows the huge basin of the stable spiral point at $b = 0.5$. This means that, whatever the initial temperature and density of the gas are, the thermodynamic state of the gas settles to an equilibrium with temperature $\sim 10^7 \text{ K}$ (for $T_0 \simeq 10^{7.5} \text{ K}$) in a finite time of the order of t_s (see equation 18). What actually happens at the threshold value b_2 is a first-order phase transition, which separates the hot phase in the cooling thermally unstable medium. Thus, one has a stable thermodynamic description for a gas with embedded cold condensations for $b \geq b_{\text{crit}} \approx 0.2$, when the oscillations are small. The occurrence of the relaxation oscillations in the vicinity of a saddle-connection follows from theorem 6.1.1 in Guckenheimer & Holmes (1983). A detailed discussion of the cooling function properties, which result in the saddle connection, can be found in Kritsuk (1992).

The key equation (16) does not contain an absolute value of the cooling, therefore one can conclude that, although the cooling is less efficient for metallicities lower than solar, the structure of equilibrium states, and, in particular, the equilibrium temperature $T(b, Z)$ does not change dramatically with Z . This is actually the case, as follows from the calculations based on the zero-field non-equilibrium ionization cooling functions of Sutherland & Dopita (1993). For the same value of T_0 as before and $Z = 0.1 Z_\odot$ the critical points, corresponding to the same catastrophic transitions, are $b_1 = 0.001$ and $b_2 = 0.097$. The Hopf bifurcation occurs somewhat earlier, at $b_3 = 0.136$. In the zero metallicity case $b_1 = 0.00048$ and $b_2 \approx 0.029$, but the nature of the saddle connection at b_2 is different [positive trace case, see

[‡] The notion of *catastrophe* is introduced in non-linear dynamics to specify a spontaneous birth of an equilibrium state at a critical point. A fold is an example of such a *discontinuous* bifurcation. Its normal form, which embodies the local low-order approximation, may be written as $\dot{x} = \mu - x^2$, where for control $\mu > 0$ a pair of equilibria exists, one attracting and the other repelling. For $\mu < 0$ the solutions diverge to $x \rightarrow -\infty$ as $t \rightarrow \infty$ (Thompson & Stewart 1989).

[§] The profound changes in qualitative behaviour of the system near the threshold value b_2 are associated solely with the *global* topological configuration of the *insets* and *outsets* (the incoming and outgoing critical trajectories) of the saddle fixed point, which requires a finite region in the phase plane and cannot be described locally. A saddle connection bifurcation is known to occur, for example, in the averaged autonomous van der Pol system [see equation (2.1.14) of Guckenheimer & Holmes (1983)].

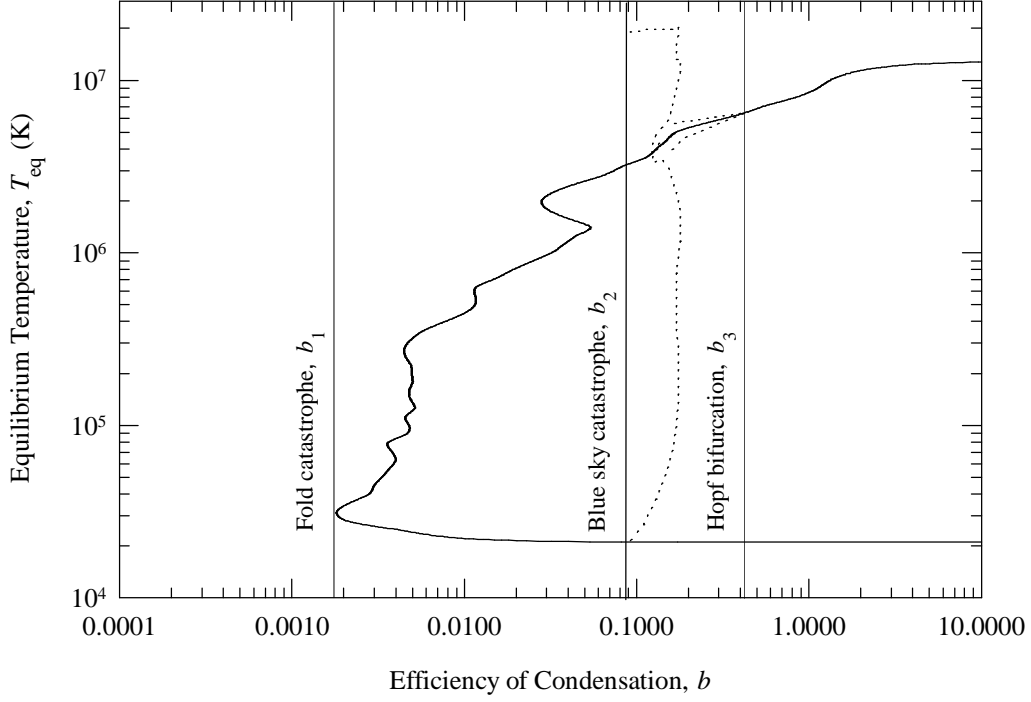


Figure 1. Bifurcation diagram for $T_0 = 3 \times 10^7$ K and $Z = Z_\odot$. The solid line shows the equilibrium temperature $T = \Theta_{\text{eq}} T_0$ as a function of condensation efficiency b . Dotted lines indicate minimum and maximum temperature values for limit cycle solutions. The phase transition occurs at $b = b_2$.

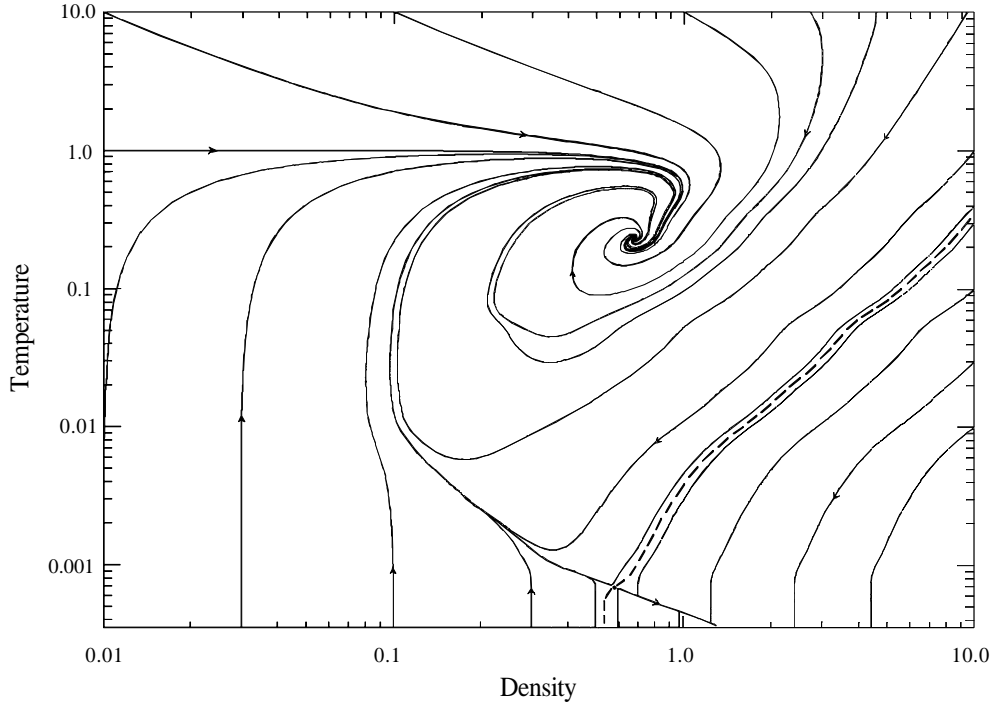


Figure 2. Phase portrait for one-zone model with $T_0 = 3 \times 10^7$ K, $b = 0.5$, and $Z = Z_\odot$. Solid lines with arrows show trajectories in the phase plane (temperature and density are dimensionless). Dashed lines indicate the insets of the *saddle* or *separatrices*, which separate the attraction domain of the stable *spiral* point.

Guckenheimer & Holmes (1983) for details], and therefore an unstable limit cycle appears before the second key bifurcation, at $b \leq b_2$. These details, however, do not change the general picture of the phase transition due to the structural stability of bifurcations involved.

The main conclusions of this subsection are the following: (i) the distributed sources and sinks of mass and energy in the hot gaseous halo may be locally balanced and the thermodynamic equilibrium is stable if $b > b_{\text{crit}}(T_0, Z)$; (ii) non-equilibrium solutions settle to the steady state from any initial conditions in its huge domain of attraction, and (iii) the equilibrium gas density is proportional to $\sqrt{\rho_*}$. It is worth emphasizing here that the phenomenon of phase transition in the system is not due to SN heating, but is due to a certain combination of the heating and distributed mass deposition.

3.4 The role of feedback

As shown in the previous subsections, the stable equilibrium can be reached by the system with no feedback heating. If star formation occurs in the condensed material, a relatively small energy feedback can modify the dynamics. This problem will be studied in detail elsewhere. Here we concentrate only on the effects that feedback heating has on the positions of the fixed points in the phase plane. It is assumed that the feedback does not alter the growth rate of condensational instability (11). Then equation (13) must be rewritten as

$$\frac{dT}{dt} = \frac{1}{\rho} \{ \alpha \rho_* (T_0 - T) + \dot{\rho}_{\text{ti}} [T_1 - (\gamma - 1)T] - \rho^2 \Lambda / c_v \}, \quad (19)$$

to account for the additional heating. The new quantity $T_1 = \varepsilon_{\text{fb}} T_{\text{fb}}$ is introduced as the feedback temperature. It is easy to check that near the equilibrium equation (19) is equivalent to (13) with $T_0 + T_1$ substituted for T_0 in equation (13). Therefore the presence of additional feedback heating does not change the structure of equilibria; only the characteristic heat source temperature increases, providing a higher equilibrium temperature for the gas. The role of feedback is somewhat more complex in situations that are far from equilibrium due to a time delay of the feedback star formation.

4 HYDROSTATIC RECYCLING OF ISOTHERMAL GAS

Perhaps 90 per cent of the papers on cooling flows contain an explanation for the flow's existence as due to a short cooling time-scale in the central region of a cluster or a group, where a cD or giant elliptical galaxy is located. It will be shown in this section that, while this condition is necessary for the flow to occur, it is not always sufficient. Note that the model discussed here is based on the same physics that is incorporated in most of the cooling flow models. The only difference is that special attention is paid to make the description more self-consistent and to incorporate the stability analysis in order to restrict the parameter space and to avoid problems in numerical simulations[¶].

[¶] For example, if non-linear relaxation oscillations of the thermodynamic state of the gas occur, special care must be taken to

4.1 Does cooling gas necessarily flow?

Simple comparison of equations (6) and (14) demonstrates that a self-consistent hydrostatic model for isothermal gas recycling in the hot corona of a giant elliptical galaxy can be constructed if

$$\beta(\sigma_*, T_0, Z, b) = \frac{1}{2}, \quad (20)$$

i.e. in the same case in which the ρ_* distribution provides the observed optical surface brightness profile (see Section 2). The gas metallicity, Z , must be uniform over the galaxy. Equation (20) can be used as an additional constraint to reduce the dimension of the parameter space of the model. For example, the definition for β (equation 5), equation (15), and the equilibrium condition (16) allow one to calculate the value of b for given T_0 , σ_* , and Z as

$$b = \left[\left(\frac{kT_0}{2\gamma\mu m_p \sigma_*^2} - 1 \right) (2 - \nu_{\text{eq}}) - 1 \right]^{-1}. \quad (21)$$

Finally, the integration constant C in equation (6) can be obtained from equation (14):

$$C = \sqrt{\frac{\alpha(c_0^2 - \gamma c^2)}{(\gamma - 1)\Lambda(T, Z)}}. \quad (22)$$

The rate of recycling is a strong function of radius and scales as $t_s^{-1} \sim \rho_*^{1/2} \sim \rho$ in the equilibrium. As the star formation rate in the cooling gas is proportional to the stellar density in the galaxy, the newly born stars and the associated heating are distributed in such a way that they do not distort the structure of existing gaseous and stellar components. Therefore the recycling is homologous.

For a comparison with cooling flow models one can formally calculate the mass deposition (accretion) rate for the recycling model as

$$\dot{M}(r) = \int_0^r 4\pi r^2 \dot{\rho}_{\text{ti}}(r) dr = \alpha M_*(r). \quad (23)$$

For $r \gg r_c$ one has $\dot{M} \sim r^{3-n}$, if $\rho_* \sim r^{-n}$, and, thus the model predicts a scaling $\dot{M} \propto r$, if the stellar density distribution is that of the isothermal sphere. Generic slopes of optical surface brightness profiles for giant elliptical galaxies are in the range from 1.65 to 2.1 (Mihalas & Binney 1981). Therefore $-0.1 \lesssim d \log \dot{M}(r) / d \log r \lesssim 0.4$. While giant ellipticals have relatively steep surface brightness profiles and correspondingly flat $\dot{M}(r)$, cDs, having flatter brightness distributions, must have steeper mass deposition profiles.

If the radiative cooling function $\Lambda(T, Z)$ is assumed to be known, the list of input parameters of the model includes the following values: $\rho_{\text{DM}0}$, ρ_* , σ_* , α , T_0 , and Z . The model could be applied in several consecutive steps. First, the ratio $(\rho_{\text{DM}0} + \rho_0) / \rho_*$ and ρ_* must be determined as the best-fitting values for the Poisson's equation solutions to adjust the optical surface brightness profile. Secondly, the temperature and metallicity, derived from the spectral analysis of the X-ray data, provide the condensation efficiency b for the assumed value of T_0 . An iterative procedure must be applied to get the value of T_0 that satisfies the observed X-ray luminosity. If the iterations converge, finally, all involved density

ensure the convergence of the numerical method in use, cf. Friaça (1993).

distributions are known and the projected distribution of the X-ray emission may be compared with the observed one.

Evidently, it is not always possible to find a hydrostatic solution that fits the observed temperature estimates $kT \geq 1.5$ keV, if the only heat source is SN Ia events with a ‘standard’ rate. If the gas inside the cooling radius is indeed so hot, there are two possible solutions of this problem: either repetitive gravitational heating is important due to violent changes in the gravitational potential of the cluster (or group) in a series of merging events, or the feedback star formation heated the gas up. To distinguish between these two or to find the proportions in which both are involved, the chemical evolution of the gaseous halo must be studied. Simple considerations for the gas enrichment in the course of hydrostatic recycling are presented in the next subsection.

The recycling model represents a special exact steady-state solution of the general time-dependent hydrodynamic problem

$$\frac{\partial \rho}{\partial t} + \nabla \cdot (\rho \mathbf{v}) = \alpha \rho_* - \dot{\rho}_{\text{ti}}, \quad (24)$$

$$\frac{\partial (\rho \mathbf{v})}{\partial t} + \nabla (\rho \mathbf{v}^2 + p) = \rho \nabla \phi - \dot{\rho}_{\text{ti}} \mathbf{v}, \quad (25)$$

$$\frac{\partial E}{\partial t} + \nabla \cdot [\mathbf{v}(E + p)] = \alpha \rho_* e_* - \dot{\rho}_{\text{ti}}(E + p)/\rho - \rho^2 \Lambda + \rho \mathbf{v} \cdot \nabla \phi + \nabla \cdot \mathbf{q}, \quad (26)$$

in which *hydrostatic* and *thermal* balance are decoupled. Here $p = (\gamma - 1)e\rho$ is the pressure, e is the specific internal energy, $e_* = c_v T_0$, the energy density $E = \rho(e + v^2/2)$, and \mathbf{q} is the heat flux. Numerical solution of equations (24)–(26) can be used to check the convective stability of the gas in the equilibrium recycling model and to study possible settling solutions in the inflow–outflow context. This requires multidimensional simulations and will be the subject of a separate paper. It is known from time-dependent numerical experiments on cooling flows that the distributed mass sink stabilizes the flow against the cooling catastrophe for a sufficiently high condensation rate (Meiksin 1988; Friaça 1993). The general mechanism of stabilization and the domain of the parameter space where it operates have been described comprehensively in Section 3 above. Thus, numerical simulations of thermally unstable gas flows *must* take into account the condensational instability. This, however, modifies the gas dynamics, because the gas becomes inelastic (Kritsuk 1994). A new type of elementary solution appears, representing a sort of subsonic condensation wave, slowly propagating in the direction opposite to the local pressure gradient and ‘reloading’ the flow. The structure of wave fronts follows the random velocity field in the gas and therefore must be filamentary. Perhaps systems of bright filaments, observed in optical emission lines in some ‘cooling flows’, could be remnants of violent non-uniform condensation events in the core of the gas distribution during post-merging transitions to hydrostatic equilibrium.

4.2 Coronal gas enrichment

The hot gas metallicity is determined by the history of stellar mass loss and supernova activity in the galaxy. Keeping the notation of Loewenstein & Mathews (1991), one can write

an equation for the i th element mass fraction $z_i = \rho_i/\rho$ in the ISM:

$$\frac{dz_i}{dt} = \frac{\rho_*}{\rho} (\alpha_* y_{*,i} + \alpha_{\text{sn}} y_{\text{sn},i} - \alpha z_i), \quad (27)$$

where $y_{*,i}$ and $y_{\text{sn},i}$ are the yields of the element, coming from stellar mass loss and SN Ia explosions, respectively. Under hydrostatic steady-state conditions equation (27) reduces to

$$z_{i,\text{eq}} = \frac{\alpha_* y_{*,i} + \alpha_{\text{sn}} y_{\text{sn},i}}{\alpha} \approx y_{*,i} + \frac{\alpha_{\text{sn}}}{\alpha} y_{\text{sn},i},$$

and therefore the metallicity of the ISM may reflect that of the stellar population with the additional contribution from supernovae. The time-scale for gas enrichment,

$$t_z = \frac{\rho}{\rho_*} \left[\alpha_* \left(\frac{y_{*,i}}{z_i} - 1 \right) + \alpha_{\text{sn}} \left(\frac{y_{\text{sn},i}}{z_i} - 1 \right) \right]^{-1}, \quad (28)$$

is proportional to the recycling time-scale t_s , if all values in square brackets do not depend on the radius. Hence, if at some moment the hydrostatic gas with uniform Z has lower abundances than the stellar matter, a negative gradient of metallicity is established in the course of evolution. It can be erased later, if the system has enough time to reach its ‘chemical’ equilibrium. This would not be the case if the stellar metallicity distribution (and, therefore, $y_{*,i}$) in the galaxy were non-uniform. There are indications, based on magnesium indices as tracers of metallicity, that, while giant elliptical galaxies are inferred to have high metallicities, their metallicity gradients are low, resulting in comparatively metal-rich stellar haloes (Thomsen & Baum 1989).

The simplified picture above does not take into account some important effects, which can alter the metallicity distribution and the absolute value of metallicity in the halo of a galaxy. First, if the enriched gas of stellar winds and supernova shells are not very well mixed into the hot IGM, but rather cool down after kinetic energy exchange with the hot medium, then there is no direct relation of the gas metallicity to the supernova rate or stellar metallicity of the galaxy. Secondly, the environmental effects could be important for gaseous haloes of dominant group/cluster members, as substructure merging in a galaxy distribution can heat the gas, and mix the enriched intragalactic medium with low-metallicity intragroup/cluster gas. While it seems to be possible to account for the first complication in the model proposed [just substituting a cooling function of higher Z in equation (11)], one has to take care in applying the model to the hotter halo of a dominant member of a potentially dynamically young aggregation of galaxies, where the gas temperature still keeps a record of the recent merging event, but not one of the current SN activity. Adjusting the thermal equilibrium condition in this case would require an unacceptably high supernova rate (and/or feedback heating) to get a higher value of T_0 .

5 DISCUSSION OF OBSERVATIONAL ISSUES

It was pointed out in Section 2 that stellar surface brightness distributions, obtained with $\beta = 1/2$, are fitted well by the $R^{1/4}$ -law. The scaling relation of the one-zone model showed that a mass deposition (star formation) rate proportional to ρ^2 allows stable recycling of the hot gas over the whole

galaxy with zero bulk motion of the gas. It will be illustrated here that the $\beta = 1/2$ model fits observed optical and X-ray surface brightness distributions well and reproduces major correlations.

5.1 X-ray surface brightness distributions

It is convenient to fit observed X-ray surface brightness distributions $\Sigma(R)$ with a simple formula, which is a generalization of the modified Hubble profile,

$$\Sigma(R) = \Sigma_0 \left[1 + \left(\frac{R}{r_c} \right)^2 \right]^{-3\beta_{\text{fit}} + 0.5} \quad (29)$$

[see, e.g., Binney & Tremaine (1987)], where Σ_0 , r_c , and β_{fit} are free parameters and R is the distance from the centre in projection. Due to the different natures of X-ray thermal emission from diffuse gas and optical stellar light, the model with $\beta = 1/2$, which implies $\rho_* \propto \rho^2$, provides optical and X-ray surface brightness distributions that match each other^{||}. Therefore, $\beta_{\text{fit}} \approx \beta_{\text{fit},*}$. This is known to be the case, as far as relatively isolated elliptical galaxies are concerned [see, for example, *Einstein* IPC and HRI data on a sample of six early-type galaxies, which includes three Virgo cluster members: NGC 4472 (M49), NGC 4636, and NGC 4649 (M60) (Trinchieri et al. 1986); *ROSAT* PSPC observations of NGC 4636 (Trinchieri et al. 1994), NGC 4365 and NGC 4382 (M85) (Fabbiano, Kim & Trinchieri 1994); analysis of optical and X-ray surface photometry of NGC 1399, the central cD galaxy in the Fornax Cluster (Killeen & Bicknell 1988)].

In order to check if this is also true for M87, the X-ray dominant galaxy in the centre of a reasonably rich cluster, the results of *ROSAT* PSPC and HRI observations were analysed and compared with optical photometry of M87 at faint light levels in the *B* and *V* bands. The optical data are available to distances of $\approx 260d_{15}$ kpc^{**} along the major axis and ≈ 90 kpc on the minor axis (Carter & Dixon 1978). The azimuthally averaged slope of the optical surface brightness profile is -1.66 and corresponds to $\beta_{\text{fit},*} = 0.44$, while β_{fit} for the averaged PSPC X-ray image is 0.45 ± 0.01 (Böhringer 1994, private communication). Analysis of the NW sector of the HRI image, which is not contaminated by the radio components, gives $\beta_{\text{fit}} = 0.45 \pm 0.01$. The comparison demonstrates a good agreement of X-ray and optical surface brightness distributions within the cooling radius, and similar orientations of the major axes of the outer optical and X-ray isocontours of M87.

The available surface brightness distributions allow one to determine the profiles of the mass deposition rate. Optical data give $\beta_{\text{fit}} = 0.42$ for the cD galaxy NGC 1399

^{||} In this notation the surface brightness of stellar light follows equation (29) with $\beta_{\text{fit},*}$ instead of β_{fit} , deprojected spatial distributions of stellar and gas mass density follow $\rho_* = \rho_{*0}[1 + x^2]^{-3\beta_{\text{fit},*}} \sim x^{-6\beta_{\text{fit},*}}$ and $\rho = \rho_0[1 + x^2]^{-3\beta_{\text{fit}}/2} \sim x^{-3\beta_{\text{fit}}}$, respectively, where $x = r/r_c$, and r_c could be different for the gas and the galaxy according to instrumental characteristics if the real core is unresolved. Note that β in (6) and β_{fit} in (29) are different values.

^{**} The distance of M87 is assumed to be 15 Mpc throughout this paper.

(Thomas et al. 1986; Killeen & Bicknell 1988; Grillmair et al. 1994), the cooling radius is known to be ~ 68 kpc (Thomas et al. 1986), and the stellar mass estimate is $M_*(68 \text{ kpc}) \simeq 10^{12} M_\odot$ (Jones & Forman 1994). Therefore, according to equation (23), $\dot{M}(r) \simeq 1.4(r/68 \text{ kpc})^{0.5} M_\odot \text{ yr}^{-1}$ for the adopted $\alpha = 4.7 \times 10^{-20} \text{ s}^{-1}$. The mass deposition estimate in this case is close to values $2.2\text{--}3.0 M_\odot \text{ yr}^{-1}$, obtained by Thomas et al. (1986) for a cooling flow model. Similarly, for M87 the cooling radius and mass estimates are nearly the same: 74 kpc (Stewart et al. 1984), and $M_*(70 \text{ kpc}) \simeq 10^{12} M_\odot$ (Jones & Forman 1994). The mean slope of the optical surface brightness distribution is -1.66 , therefore $\dot{M}(r) \simeq 1.4(r/70 \text{ kpc})^{0.34} M_\odot \text{ yr}^{-1}$. In this case the power index and the absolute value of the mass deposition rate disagree with the estimate, based on the ‘standard’ cooling flow analysis of *Einstein* observations: $\dot{M}(r) \simeq 10(r/70 \text{ kpc})^{2/3} M_\odot \text{ yr}^{-1}$, for $5 \lesssim r \lesssim 70$ kpc (Stewart et al. 1984). However, within the field of view of the *Einstein* Observatory SSS (~ 3 arcmin in radius) and FPCS (3 arcmin \times 30 arcmin) our result $\dot{M}(3 \text{ arcmin} \simeq 13.1 \text{ kpc}) \simeq 0.8 M_\odot \text{ yr}^{-1}$ is in rough agreement with the upper estimates neglecting heating: $\dot{M}_{\text{SSS}} \simeq 2.3 M_\odot \text{ yr}^{-1}$ (Mushotzky & Szymkowiak 1988) and $\dot{M}_{\text{FPCS}} \simeq 1.6 \pm 0.3 M_\odot \text{ yr}^{-1}$ (Canizares et al. 1982), which have been accordingly rescaled.

5.2 X-ray gas temperatures

When thermal instabilities occur in an accretion flow, two different spectral components are present in thermal X-ray emission, corresponding to terms $\dot{\rho}_{\text{ti}}e$ (conventionally, softer X-rays from *isobarically* cooling comoving gas) and $\rho^2\Lambda$ (harder emission from the diffuse gas component) in equation (26). The spectral emissivity of such a composition is

$$\epsilon_\nu(r) = \rho^2(r)\Lambda_\nu(T) + \dot{\rho}_{\text{ti}}(r)c_\nu\Gamma_\nu(T), \quad (30)$$

where

$$\Gamma_\nu(T) \equiv \frac{\gamma}{\gamma - 1} \int_0^T \frac{\Lambda_\nu(T)}{\Lambda(T)} dT \quad (31)$$

(White & Sarazin 1987b). If the gas drops out due to thermal instability in equilibrium with stellar mass loss in the hot hydrostatic halo of a galaxy, the relative contributions from cooling diffuse gas and cooling condensates are fixed by the equilibrium conditions, and have similar spatial distributions. In this case equation (30) can be transformed into

$$\epsilon_\nu(r) \propto \rho_*(r)\Lambda_\nu(T) \left[1 + q \frac{\Lambda}{T\Lambda_\nu} \Gamma_\nu(T) \right], \quad (32)$$

where for the adopted deposition law

$$q = \frac{b(2 - \nu_{\text{eq}})}{b + 1}. \quad (33)$$

The radiative cooling function in equations (30) and (31) must take into account non-equilibrium ionization effects for temperatures less than several 10^6 K (see, e.g., Sutherland & Dopita 1993).

While the idea of distributed mass deposition in cooling flows is widely exploited in physical models (Thomas 1986; White & Sarazin 1987a; Sarazin & Ashe 1989; Meiksin 1988; Meiksin 1990; David et al. 1990; Friaça 1993), analysis of observed spectra is usually based on one- or two-temperature

fits, which appear to be satisfactory, mainly due to the limited spectral resolution of the available detectors. This technique does not account for the emission of cooling condensates, and temperature estimates, based on spectral information, suffer from limited spectral and spatial resolution of the detectors, model-dependent deprojection procedures, uncertain abundances (and their gradients) in the hot ISM, and unknown H I column densities.

Emission from condensates exceeds the diffuse emission at energies below ~ 2 keV when the background temperature is 10^8 K, and below ~ 0.8 keV when the background temperature is 10^7 K (White & Sarazin 1987b). In the case of the *ROSAT* PSPC detector it will make a substantial contribution to the harder energy band of the detector, due to a blend of iron L-shell lines, if the gas condensations cool down from a temperature of about $3-4 \times 10^7$ K. In contrast, for background temperatures lower than $\sim 10^7$ K, the dominant contribution from *isobaric* cooling will be in the softer energy band. If spectral analysis does not take into account the emission from cooling condensations, the resulting pressure (and gravitating mass) estimates could contain errors of up to a factor of $\sim 2-3$. Consequently, the observational estimate of $\beta_{\text{spec}} = \sigma_*^2/(kT/\mu m_p)$ is uncertain by the same factor.

Reanalysis of the *Einstein* IPC, HRI, FPCS, and SSS observations of M87 has demonstrated the disagreement of single-phase models with mass determinations based on the optical data, while the available X-ray data are explained well (Tsai 1994a). The total enclosed mass, derived from the model at $r < 10$ arcmin [i.e. right in the central ‘cooling flow’ region, where the gas temperature drops (Böhringer et al. 1994; Nulsen & Böhringer 1995) to values lower than the $kT = 2.05 \pm 0.16$ keV determined by *Ginga* (Koyama, Takano & Tawara 1991)], falls well below the mass estimate from the optical data. The multiphase model adequately explains the X-ray data and predicts total masses, which agree with optical measurements (Tsai 1994b). The central gas temperature for this model is about 1.8×10^7 K. It seems that the main root of the problem is the lack of self-consistency in the standard procedure implemented for the gravitating mass determination in the ‘cooling flow’ region, which is based on the hydrostatic assumption on the one hand and does not account for the distributed mass deposition (as the only means to keep the thermally unstable cooling medium hydrostatic) on the other hand. The best-fitting multiphase model of Tsai (1994b) does not show any dramatic decrease of the temperature near the centre (which is typical for cooling flow models), but shows only a modest positive temperature gradient, $d \log T/d \log r = 0.114$, which is much smaller than that of the electron number density ($d \log n_e/d \log r = -0.491$ in the core of radius $r_c = 6.64$ kpc and -1.36 at $r \gg r_c$). This can be considered as an argument in favour of the isothermal approximation, adopted above, and justifies the usage of equation (2) for gravitating mass estimates.

5.3 X-ray gas metallicity

The distribution of iron abundance, as follows from the *Ginga* observation of the Virgo Cluster, gives a mean value for the central region within 1° of M87 of $Z \sim 0.5 Z_\odot$. Because the angular profile of the abundance distribution

is comparable to that of the *Ginga* collimator response (1°), the detailed structure remains unresolved. *Broad Band X-Ray Telescope* (BBXRT) observations of the interstellar medium in NGC 1399 indicated a mild positive temperature gradient ($kT = 1.0 - 1.1$ keV for the central pixel of 4 arcmin in diameter and $kT = 1.1 - 1.2$ keV for the outer pixels at ~ 7 arcmin from the centre) and a subsolar metallicity with a negative gradient on the same scale, although the statistical uncertainties do not preclude a constant metallicity (Serlemitsos et al. 1993).

Spatially resolved spectra, obtained with the *ROSAT* PSPC, can provide information on possible abundance gradients in the hot gas. Rapidly cooling regions in the centres of ‘cooling flows’ in NGC 1399 and NGC 4472 show an apparent trend of decreasing abundance with increasing radial distance (by a factor of ~ 2 for a scale of ~ 70 kpc), when T , Z , and the hydrogen column density, N_H , are treated as free parameters for the spectral fitting procedure (Forman et al. 1993; Jones & Forman 1994). If N_H is held fixed, then the gradient is smaller (Forman et al. 1993). Similarly ambiguous results were obtained by Trinchieri et al. (1994) in their detailed study of *ROSAT* PSPC data on NGC 4636. If uniform 100 per cent cosmic abundances were assumed then two-temperature components were required to fit the observed spectra; if 20 per cent abundances were assumed then one component provided a fit of the same quality. New data from the *Advanced Satellite for Cosmology and Astrophysics* (ASCA) have confirmed the lower abundances for NGC 4636, however, with a mild negative gradient: from ~ 0.3 at $R_e \simeq 8.4$ kpc to less than ~ 0.2 of the solar value at $5R_e$ (Mushotzky et al. 1994). Also there is good agreement between *ROSAT* and *ASCA* temperature profiles, $T \propto r^{0.2}$ over a scale of ~ 30 kpc (Trinchieri et al. 1994). Even lower metal abundances, $Z \sim 0.15 Z_\odot$, measured with *ASCA* were reported for NGC 1404 and NGC 4374 by Loewenstein et al. (1994).

Although the observations do not give reliable information on the metallicity distribution in hot coronae, an assumption of uniform abundances with solar ratios, adopted above, could be an appropriate zero approximation for the region inside the cooling radius. Very low metal abundances detected by *ASCA* together with typical temperatures $kT \sim 0.75$ keV would imply incomplete mixing of gas injected by SNe. However, spectral fits based on the multiphase gas model are needed to confirm the low abundance estimates.

5.4 L_X-L_B correlation

Using simple geometrical arguments, the scaling relation of the one-zone model (14), and the virial condition $\rho_0 r_c^2 = 9\sigma_*^2/4\pi G$ [see, e.g., Binney & Tremaine (1987)], one can write $L_X \propto \rho_0^2 \Lambda r_c^3 \propto \rho_* c_0^2 r_c^3 \propto \rho_* \sigma_*^2 r_c^3 \propto \sigma_*^4 r_c$. For galaxies on the fundamental plane $L_B \propto \sigma_*^{1.3} r_c$ (Djorgovski & de Carvalho 1990), therefore $L_X \propto L_B^{3.1} r_c^{-2.1}$. Using the Faber–Jackson law for bright ellipticals [$\sigma_* \propto L_B^{0.25}$ (Faber & Jackson 1976)] and the above relationship for the fundamental plane, it is easy to eliminate r_c and get $L_X \propto L_B^{1.7}$. Note that the Faber–Jackson relation can be derived from a simple self-regulated star formation scenario for a massive ($M \geq 10^{11} M_\odot$) spheroidal system (Lin & Murray 1992). This scenario implies the initial expulsion of gas, combined

with that resulting from later stellar evolution, which may form a source of gas, feeding the hot haloes of individual galaxies. In agreement with this, observations show that the relation depends on the galaxy luminosity. While for the brightest ($M_B \lesssim -20$) ellipticals $L_B \propto \sigma_*^{4.2 \pm 0.9}$, for the less luminous ones ($M_B \gtrsim -20$) the deviations from the Faber–Jackson law may be considerable: $L_B \propto \sigma_*^{2.4 \pm 0.9}$ (Davies et al. 1983). Thus, one has $L_X \propto L_B^{1.65}$ and $L_X \propto L_B^{2.15}$ for bright and faint ellipticals, respectively. These results can be compared with $L_X \propto L_B^{1.7 \pm 0.3}$ (Canizares, Fabbiano & Trinchieri 1987) and $L_X \propto L_B^{2.18 \pm 0.20}$ (Donnelly, Faber & O’Connell 1990). Note that the derived relation of X-ray to optical luminosities is quite different from the naive scaling $L_X \propto L_B$ for SN-heating dominated models.

In the framework of the recycling model the deviations from the ‘mean’ X-ray to optical luminosity relationship [the observed rms residuals of $\log L_X$ are $0.33 - 0.35$ (Donnelly et al. 1990)] may be attributed to the combined effects of: (i) galaxy-to-galaxy differences in the spectra of perturbations, which stimulate thermal instabilities in the hot gas; (ii) different rates of SN activity and/or stellar mass loss rates; (iii) variations of the chemical composition of the hot gas. Each of these circumstances determines the equilibrium gas content of a galaxy and most of them may be environmentally influenced (see also Section 5.6 below). The most dramatic deviations may occur if the efficiency of condensation b becomes lower than its critical value b_{crit} . This could stimulate oscillations of the gas density with amplitude ~ 5 (Kritsuk 1992) and, therefore, initiate the random walk of a galaxy about the mean value of L_X . The possibility of such destabilization is one of the natural explanations for considerable scatter in the $\log L_X - \log L_B$ plane.

5.5 L_X – T correlation

For the β -model $T \propto \sigma_*^2$ and therefore, using the $L_X - L_B$ relation above and the Faber–Jackson law, one obtains $L_X \propto T^{3.4}$. For the high- and low-luminosity ellipticals $L_X \propto T^{3.44}$ and $L_X \propto T^{2.54}$, respectively. Note that this scaling relation is similar to $L_X \propto T^{3.3}$, for a sample of galaxy clusters observed by *Ginga* (Arnaud 1994). For cluster cooling flows the observed X-ray luminosity–temperature relation has the same scaling, but depends also on the mass deposition rate (estimated with the ‘standard’ cooling flow analysis technique): $L_X \propto T^{3.3} \dot{M}^{0.4}$ (Fabian et al. 1994).

5.6 Gas content and environmental effects

The relation of the SN-associated heat source temperature T_0 to the equilibrium gas temperature and density, as well as Z and b , is illustrated here in Table 1, computed using equations (15), (16) and (22) and the cooling functions of Sutherland & Dopita (1993). It shows that higher metallicities result in lower T_0 values and lower gas densities (X-ray luminosities) for a fixed temperature of the hot diffuse component of the ISM. Also the higher condensation efficiency provides a lower L_X . When the efficient feedback star formation is triggered by the recent merging event, a higher equilibrium X-ray luminosity is expected. This might be the generic case for dominant galaxies in rich and, therefore, more active environments. In relatively isolated galaxies,

Table 1. Thermodynamic equilibria for hot coronal gas.

$Z = Z_\odot$						
T_{07}	$b = 0.5$		$b = 0.7$		$b = 0.9$	
	T_7	C_{-15}	T_7	C_{-15}	T_7	C_{-15}
2.0	0.54	3.34	0.57	3.30	0.60	3.25
2.5	0.61	3.95	0.65	3.83	0.70	3.71
3.0	0.69	4.38	0.76	4.20	0.82	4.05
3.5	0.77	4.73	0.99	4.26	1.16	4.03
4.0	1.06	4.71	1.27	4.57	1.35	4.51
4.5	1.29	5.13	1.40	5.08	1.47	5.01
5.0	1.40	5.63	1.52	5.55	1.60	5.46
5.5	1.50	6.10	1.64	5.97	1.75	5.83
6.0	1.60	6.52	1.79	6.33	1.89	6.21
7.0	1.85	7.26	2.02	7.10	2.12	6.97
8.0	2.04	7.99	2.21	7.79	2.36	7.57
9.0	2.21	8.65	2.47	8.30	2.62	8.09
10.	2.43	9.16	2.68	8.84	2.83	8.63

$Z = 0.32 Z_\odot$						
T_{07}	$b = 0.5$		$b = 0.7$		$b = 0.9$	
	T_7	C_{-15}	T_7	C_{-15}	T_7	C_{-15}
2.0	0.52	4.52	0.57	4.41	0.60	4.32
2.5	0.61	5.25	0.66	5.10	0.70	4.97
3.0	0.69	5.86	0.76	5.60	0.85	5.30
3.5	0.79	6.28	0.94	5.84	1.02	5.64
4.0	0.95	6.53	1.13	6.15	1.27	5.88
4.5	1.13	6.83	1.31	6.56	1.37	6.47
5.0	1.30	7.24	1.40	7.13	1.51	6.87
5.5	1.38	7.78	1.56	7.43	1.64	7.27
6.0	1.50	8.18	1.66	7.88	1.73	7.77
7.0	1.69	8.98	1.84	8.71	2.02	8.30
8.0	1.87	9.71	2.12	9.21	2.25	8.98
9.0	2.11	10.2	2.33	9.81	2.50	9.48
10.	2.29	10.8	2.55	10.3	2.68	10.1

The heat source temperature T_{07} and the equilibrium gas temperature T_7 are given in units of 10^7 K. The integration constant C_{-15} in equation (6) is computed for the stellar mass loss rate $\alpha = 4.7 \times 10^{-20} \text{ s}^{-1}$ and given in units of $10^{-15} (\text{g cm}^{-3})^{\frac{1}{2}}$.

as is illustrated in the following, the standard value of the SN rate can readily explain the observed gas temperatures. Note, however, that the uncertainties of the T_0 estimates inherit the uncertainties of the model cooling functions and their first derivatives. Therefore the values of T_0 may be only 30–50 per cent accurate.

Recent *ASCA* observations of bright elliptical galaxies in the Virgo Cluster revealed hard X-ray components with colour temperature $kT \geq 2$ keV in addition to extended thermal X-ray emission of temperature $kT \sim 1$ keV (Matsushita et al. 1994). This hard component is primarily attributed to the integrated emission from discrete X-ray sources, associated with the optical galaxy. For galaxies located in the area of extended cluster X-ray emission, the discrete sources alone cannot account for all the hard X-ray flux detected with *ASCA*. It was assumed, therefore, that the hard components of NGC 4406 (M86) and NGC 4374 (M84) are contaminated by the foreground/background Virgo intracluster medium emission. In the case of NGC 4472 the hard-band image is elongated and displaced from the optical galaxy and from the soft-band image as well. This is interpreted as the locally enhanced ICM emission plus the

discrete-source contribution, although their respective contributions remain unspecified. The temperature of the soft emission from NGC 4472, $kT = 0.83 \pm 0.04$ keV, corresponds to an SN heating temperature $T_0 \approx 3.4 \times 10^7$ K for the observed metallicity $Z \sim 0.42 Z_\odot$ and the condensation efficiency $b = 0.7$. For NGC 4636 located at the outskirts of the Virgo Cluster, *ROSAT* PSPC data imply a similar hard ($kT > 0.9$ keV) component, which is more extended than the soft one ($kT \simeq 0.6 - 0.8$ keV) and probably is not directly related to the galaxy. However, this is only true if 100 per cent cosmic abundances are assumed. With 20 per cent cosmic abundances only one temperature component ($kT \simeq 0.6 - 1.0$ keV) is required for spectral fits (Trinchieri et al. 1994).

The *BBXRT* data for NGC 1399, a cD galaxy in a poor cluster, suggest a gas temperature $kT = 1.0 - 1.2$ keV and metallicities of about $0.5 Z_\odot$ with large uncertainties (Serlemitsos et al. 1993). The analysis of two-temperature models revealed (similarly to the Virgo galaxies) a hard component of X-ray emission with $kT \sim 6$ keV and provided a lower temperature ~ 1 keV and a higher metallicity $0.76 Z_\odot$ for the primary soft component. This would imply a characteristic heat source temperature $T_0 \approx 4 \times 10^7$ K.

An accurate deprojection analysis of the *ROSAT* PSPC spectral data on M87 provided temperature estimates for the centre of the ‘cooling flow’ region ($r \leq 3.33$ arcmin $\simeq 15$ kpc) of $kT = 1.1 - 1.4$ keV (Nulsen & Böhringer 1995). Such a temperature would require $T_0 \approx 5 \times 10^7$ K for the sub-solar metallicity $Z \sim 0.5 Z_\odot$ and an even lower value for solar metallicity. The condensation efficiency $b = 0.7$ roughly corresponds to $q = 0.874$ – the value for the best-fitting multiphase model of Tsai (1994b), see equation (33). Note that the temperature estimate was made in Nulsen & Böhringer (1995) for the region where the errors due to contamination by the ICM emission are small. The straightforward approach would require $T_0 \sim 9 \times 10^7$ K for the gas temperatures detected with wide-beam instruments [e.g. $kT \sim 2$ keV, *Ginga* (Koyama et al. 1991)]. Note, however, that the multiphase model based on *Einstein* data gives a central temperature estimate of $T \simeq 1.8 \times 10^7$ K.

Although in all three cases discussed above the low gas temperature estimates were obtained on the basis of a single-phase description, if they are considered as rough estimates for the temperature of the diffuse component of the cooling gas, the standard SN Ia rate appears to be sufficient for thermodynamic equilibrium at the measured temperatures. The analysis of *ASCA* observations, based on the multiphase model, would help to check whether the diffuse component of the multiphase ISM in central dominant galaxies actually has a low temperature $\lesssim 1$ keV and nearly solar metallicity. In this case a $kT \lesssim 1$ keV galactic atmosphere might be embedded in the extended intracluster gas with a higher temperature and lower metallicity. *ASCA* data on NGC 4696/Centaurus lend support to this option (Fukazawa et al. 1994). Such a complex quasi-hydrostatic configuration can be described with a hybrid model, including the recycling interior of the dominant galaxy matched at the cooling radius [where $t_c(r_{\text{cool}}) = H_0^{-1}$] with an isothermal β -model for the hotter tenuous intracluster gas. If the ratio of the stellar-to-gas mass is low and the cooling radius is larger than the extent of the optical galaxy, then a cooling flow is unavoidable. It starts from the cooling radius, enters the

galaxy, and disappears, providing material for star formation.

6 CONCLUSIONS

A purely hydrostatic model for the hot gas in normal elliptical galaxies has been presented as an alternative to the ‘standard’ cooling flow picture. The model independently develops an option suggested by Thomas et al. (1986) that perhaps there are no radial gas flows, so that all gas present at some radius originated there (e.g. from stellar mass loss) and cools and is deposited *in situ*. Energy injection from SNe and feedback heating due to star formation from deposited material have been also incorporated in the description of equilibrium gas recycling. Formally, the model is quite similar to the steady-state cooling flow formulation of Sarazin & Ashe (1989) but with zero bulk motion of the gas. (Note that the notion of the cooling flow itself implies highly subsonic velocities and there are no observational data that would directly confirm the existence of the *flow*.) Therefore, the recycling model, representing a ‘minimal cooling flow’, gives the exact lower estimates of the mass deposition rate in elliptical galaxies and fills the gap in a family of models for hot gaseous coronae, being a fully self-consistent hydrostatic model which for the first time takes into account the whole set of sources and sinks of mass and energy. It has the advantage of an analytical description of gas equilibria, which allows the study of their linear stability. However, the global thermal-convective stability of such a hydrostatic recycling atmosphere of a galaxy must be the subject of a separate numerical investigation.

Summarizing the results of this study, it is worthwhile to stress that the galaxy, located in the centre of the cooling region, may play an important role, providing a complex mechanism for hydrostatic support of thermally unstable gas. The moderate amount of SN Ia heating in combination with the distributed mass sink is able to compensate the radiative cooling and the stellar mass loss in such a way that quasi-isothermal hot gas is kept in both *hydrostatic* and *thermodynamic* equilibrium. The latter becomes possible due to a first-order phase transition, which separates the stable hot gas phase for a sufficiently high efficiency of condensation. Having no energy input and/or mass sink it is impossible to avoid a cooling catastrophe in the centre of the ‘cooling flow’ region, where radiative cooling and stellar mass loss are efficient.

ACKNOWLEDGMENTS

This work has been supported in part by the Russian Foundation of Fundamental Research (project code 93-02-02957) and by a grant of the American Astronomical Society. The author is grateful to Andi Burkert, Makoto Hattori, and Ewald Müller for helpful comments on the manuscript and to the staff of MPA and MPE for the warm hospitality.

REFERENCES

- Anders E., Grevesse N., 1989, *Geochim. Cosmochim. Acta*, 53, 197

- Arnaud M., 1994, in Zeitter W.C., ed., Proc. NATO ASI, Cosmological Aspects of X-Ray Clusters of Galaxies. Series C: Math. and Phys. Sci., vol. 441, Kluwer, Dordrecht, p. 197
- Binney J., Tremaine S., 1987, Galactic Dynamics. Princeton Univ. Press, Princeton
- Böhringer H., Briel U.G., Schwarz R.A., Voges W., Hartner G., Trümper J., 1994, Nat, 368, 828
- Burke J.R., Silk J., 1974, ApJ, 190, 1
- Burkert A., 1994, Reviews in Modern Astronomy, vol. 7. Astron. Ges., Hamburg, p. 191
- Canizares C.R., Clark G.W., Jernigan J.C., Markert T.H., 1982, ApJ, 262, 33
- Canizares C.R., Fabbiano G., Trinchieri G., 1987, ApJ, 312, 503
- Carter D., Dixon K.L., 1978, AJ, 83, 574
- Cavaliere A., Fusco-Femiano R., 1976, A&A, 49, 137
- Ciotti L., D'Ercole A., Pellegrini S., Renzini A., 1991, ApJ, 376, 380
- David L.P., Forman W., Jones C., 1990, ApJ, 359, 29
- Davies R.L., Efstathiou G., Fall S.M., Illingworth G., Schechter P.L., 1983, ApJ, 266, 41
- Djorgovski S., de Carvalho R., 1990, in Fabbiano G., Gallagher J.S., Renzini A., eds, Proc. Workshop of the Advanced School of Astronomy, Windows on Galaxies. Kluwer, Dordrecht, p. 9
- Donnelly R.H., Faber S.M., O'Connell R.M., 1990, ApJ, 354, 52
- Fabbiano G., Kim D.-W., Trinchieri G., 1994, ApJ, 429, 94
- Faber S.M., Gallagher J.S., 1976, ApJ, 204, 365
- Faber S.M., Jackson R.E., 1976, ApJ, 204, 668
- Fabian A.C. 1994, ARA&A, 32, 277
- Fabian A.C., Nulsen P.E.J., Canizares C.R., 1984, Nat, 310, 933
- Fabian A.C., Crawford C.S., Edge A.C., Mushotzky R.F., 1994, MNRAS, 267, 779
- Forman W., Jones C., Tucker W., 1985, ApJ, 293, 102
- Forman W., Jones C., David L., Franx M., Makishima K., Ohashi T., 1993, ApJ, 418, L55
- Friaza A.C.S., 1993, A&A, 269, 145
- Fukazawa Y., Ohashi T., Fabian A.C., Canizares C.R., Ikebe Y., Makishima K., Mushotzky R.F., Yamashita K., 1994, PASJ, 46, L55
- Grillmair C.J., Freeman K.C., Bicknell G.V., Carter D., Couch W.J., Sommer-Larsen J., Taylor K., 1994, ApJ, 422, L9
- Guckenheimer J., Holmes Ph., 1983, Nonlinear Oscillations, Dynamical Systems, and Bifurcations of Vector Fields. Springer Verlag, New York
- Hattori M., Habe A., Ikeuchi S., 1987, Prog. Theor. Phys., 78, 1099
- Jones C., Forman W., 1994, Preprint CfA
- Killeen N.E.B., Bicknell G.B., 1988, ApJ, 325, 165
- Koyama K., Takano S., Tawara Y., 1991, Nat, 350, 135
- Kritsuk A.G., 1992, A&A, 261, 78
- Kritsuk A.G., 1994, in Zeitter W.C., ed., Proc. NATO ASI, Cosmological Aspects of X-Ray Clusters of Galaxies. Series C: Math. and Phys. Sci., vol. 441, Kluwer, Dordrecht, p. 189
- Lin D.N.C., Murray S.D., 1992, ApJ, 394, 523
- Loewenstein M., Mathews W.G., 1991, ApJ, 373, 445
- Loewenstein M., Mushotzky R.F., Tamura T., Ikebe Y., Makishima K., Matsushita K., Awaki H., Serlemitsos P.J., 1994, ApJ, 436, L75
- Mathews W.G., 1990, ApJ, 354, 468
- Matsushita K. et al., 1994, ApJ, 436, L41
- Meiksin A., 1988, ApJ, 334, 59
- Meiksin A., 1990, ApJ, 352, 466
- Mihalas D., Binney J., 1981, Galactic Astronomy, Second edn. W.Freeman & Co, New York
- Mushotzky R.F., Szymkowiak A.E., 1988, in Fabian A.C., ed., Proc. NATO ASW, Cooling Flows in Clusters and Galaxies. Series C: Math. and Phys. Sci., Kluwer, Dordrecht, p. 53
- Mushotzky R.F., Loewenstein M., Awaki H., Makishima K., Matsushita K., Matsumoto H., 1994, ApJ, 436, L79
- Navarro J.F., Frenk C.S., White S.D.M., 1995, MNRAS, 275, 720
- Nulsen P.E.J., 1986, MNRAS, 221, 377
- Nulsen P.E.J., Böhringer H., 1995, MNRAS, 274, 1093
- Sarazin C.L., Ashe G.A., 1989, ApJ, 345, 22
- Sarazin C.L., White R.E., III, 1987, ApJ, 320, 32
- Serlemitsos P.J., Loewenstein M., Mushotzky R.F., Marshall F.E., Petre R., 1993, ApJ, 413, 518
- Silk J., Djorgovski S., White R.F.G., Brusual A., 1986, ApJ, 307, 415
- Stewart G.C., Canizares C.R., Fabian A.C., Nulsen P.E.J., 1984, ApJ, 278, 536
- Sutherland R.S., Dopita M.A., 1993, ApJS, 88, 253
- Thomas P.A., 1986, MNRAS, 220, 949
- Thomas P.A., Fabian A.C., Arnaud K.A., Forman W., Jones C., 1986, MNRAS, 222, 655
- Thompson J.M.T., Stewart H.B., 1989, Nonlinear Dynamics and Chaos. John Wiley & Sons, Chichester
- Thomsen B., Baum W.A., 1989, ApJ, 347, 214
- Turatto M., Cappellaro E., Benetti S., 1994, AJ, 108, 202
- Trinchieri G., Fabbiano G., Canizares C.R., 1986, ApJ, 310, 637
- Trinchieri G., Kim D.-W., Fabbiano G., Canizares C.R., 1994, ApJ, 428, 555
- Tsai J.C., 1994a, ApJ, 423, 143
- Tsai J.C., 1994b, ApJ, 429, 119
- van den Bergh S., Tammann G.A., 1991, ARA&A, 29, 363
- White R.E., III, Sarazin C.L., 1987a, ApJ, 318, 612
- White R.E., III, Sarazin C.L., 1987b, ApJ, 318, 621

This paper has been produced using the Royal Astronomical Society/Blackwell Science L^AT_EX style file.